Published for SISSA by Springer

Received: May 5, 2019
Accepted: July 25, 2019
Published: August 21, 2019

Collider constraints on Z′ models for neutral current B-anomalies

B.C. Allanach,[a] **J.M. Butterworth**[b] **and Tyler Corbett**[c,1]

[a] *DAMTP, University of Cambridge, Wilberforce Road, Cambridge, CB3 0WA, United Kingdom*
[b] *Department of Physics & Astronomy, University College London, Gower St, London, WC1E 6BT, United Kingdom*
[c] *The Niels Bohr International Academy, University of Copenhagen, Blegdamsvej 17, Copenhagen, DK-2100, Denmark*

E-mail: B.C.Allanach@damtp.cam.ac.uk, j.butterworth@ucl.ac.uk, corbett.t.s@gmail.com

Abstract: We examine current collider constraints on some simple Z' models that fit neutral current B-anomalies, including constraints coming from measurements of Standard Model (SM) signatures at the LHC. The 'MDM' simplified model is not constrained by the SM measurements but *is* strongly constrained by a 139 fb^{-1} 13 TeV ATLAS di-muon search. Constraints upon the 'MUM' simplified model are much weaker. A combination of the current B_s mixing constraint and ATLAS' Z' search implies $M_{Z'} > 1.2$ TeV in the Third Family Hypercharge Model example case. LHC SM measurements rule out a portion of the parameter space of the model for $M_{Z'} < 1.5$ TeV.

Keywords: Beyond Standard Model, Heavy Quark Physics

ArXiv ePrint: 1904.10954

[1] Corresponding author.

https://doi.org/10.1007/JHEP08(2019)106

Contents

JHEP08(2019)106

1 Introduction

Data involving the effective Lagrangian operator $b\bar{s}\mu^+\mu^-$ are currently disagreeing with Standard Model (SM) predictions. Each individual measurement typically disagrees at the 2–3σ level and over many measurements, a coherent picture is emerging. In particular $R_{K^{(*)}} \equiv BR(B \to K^{(*)}\mu^+\mu^-)/BR(B \to K^{(*)}e^+e^-)$ are predicted to be 1.00 in the SM, for lepton invariant mass squared bin $m_{ll}^2 \in [1.1, 6]\,\text{GeV}^2$. In this bin, current LHCb measurements [1, 2] imply $R_K = 0.846^{+0.060+0.016}_{-0.054-0.014}$ and $R_{K^*} = 0.69^{+0.11}_{-0.07} \pm 0.05$. The branching ratio $B_s \to \mu^+\mu^-$ [3–6] is also measured to be lower than the SM prediction, which should be accurate to the percent level. Angular distributions in the $B \to K^{(*)}\mu^+\mu^-$ decays have [7–10] a higher level of disagreement with SM predictions [11, 12], although here theoretical uncertainties in the SM prediction are significant. There are several other indications of disagreements between SM predictions and measurements and broadly speaking, the data are consistent with a beyond-the-SM (BSM) contribution to the $b\bar{s}\mu^+\mu^-$ vertex [13–20]. We call these disagreements between measurements and SM predictions the Neutral Current B-Anomalies (NCBAs). Measurements of relevant quantities from Belle II with different systematic uncertainties are eagerly awaited [21], as are updates from the LHC experiments.

The operators giving BSM contributions favoured by fits to the flavour data are

$$\mathcal{L}_{bs\mu\mu} = (\overline{b_L}\gamma^\mu s_L)(C_{LL}\overline{\mu_L}\gamma_\mu\mu_L + C_{LR}\overline{\mu_R}\gamma_\mu\mu_R) + \text{H.c.}, \tag{1.1}$$

where C_{LL} and C_{LR} are Wilson coefficients, with dimensions of inverse mass squared. There have been several global fits of such BSM operators that explain recent data involving $\bar{b}s\bar{\mu}\mu$: [22–27]. Details of the fit methodology and results vary, but they all find that a fit involving $C_{LL} \neq 0$ and $C_{LR} \in [-C_{LL},\ C_{LL}]$ can provide a significant improvement over a poor fit to the SM. There is evidence against sizeable BSM operators involving b_R and s_R in the global fits. For definiteness, we shall use the results of the fit of ref. [25]. There, $C_{LL} \neq 0$ only provides a good fit to NCBA data (6.5σ better than the SM prediction). A vector-like coupling (i.e. $C_{LL} = C_{LR}$) to muons is a 5.8σ better fit than the SM at the best-fit point, whereas an axial coupling ($C_{LL} = -C_{LR}$) coupling to muons is 5.6σ better than the SM at the best-fit point.

At tree-level, a BSM contribution to C_{LL} or C_{LR} can come from leptoquarks and/or Z's, either of which must have flavour dependent couplings. Here, we shall focus on the Z' possibility. Many models based on spontaneously broken flavour-dependent gauged U(1) symmetries [28, 29] have been proposed from which such Z's may result, for example from $L_\mu - L_\tau$ and related groups [28, 30–62]. Some models also have several abelian groups [63] leading to multiple Z's. Some other models [64, 65] generate the $b\bar{s}\mu^+\mu^-$ operator with a loop-level penguin diagram.

In ref. [66], Run I di-jet and di-lepton resonance searches (and early Run II searches) were used to constrain simple Z' models that fit the NCBAs. In refs. [62, 67], the sensitivity of future hadron colliders to Z' models that fit the NCBAs was estimated. A 100 TeV future circular collider (FCC) [68] would have sensitivity to the whole of parameter space for one model (MDM) and the majority of parameter space for another (MUM). However, given recent updates on LHC Z' searches released by the ATLAS experiment and on the NCBAs, it seems that the time is ripe for a fresh analysis of the resulting constraints upon Z' models that fit the NCBAs.

ATLAS has released 13 TeV 36.1 fb^{-1} $Z' \to t\bar{t}$ searches [69, 70], which impose $\sigma \times BR(Z' \to t\bar{t}) < 10\,\text{fb}$ for large $M_{Z'}$. There is also a search [71] for $Z' \to \tau^+\tau^-$ for 10 fb^{-1} of 8 TeV data, which rules out $\sigma \times BR(Z' \to \tau^+\tau^-) < 3\,\text{fb}$ for large $M_{Z'}$. These searches constrain, in principle, some of the flavourful Z' models that we introduce below, but they produce less stringent constraints upon the models that we study than an ATLAS search for $Z' \to \mu^+\mu^-$ in 139 fb^{-1} of 13 TeV pp collisions [72]. We shall therefore concentrate upon this search, recasting it for some models that solve the NCBAs. The constraints are in the form of upper limits upon the fiducial cross-section σ times branching ratio to di-muons $BR(Z' \to \mu^+\mu^-)$ as a function of $M_{Z'}$. At large $M_{Z'} \approx 6\,\text{TeV}$, $\sigma \times BR(Z' \to \mu^+\mu^-) < 0.015\,\text{fb}$ [73] and indeed this will prove to be the most stringent Z' direct search constraint (being stronger than the others mentioned above) on the models which we study.

In section 2, we introduce simplified models Z' which can provide a good fit to the NCBAs, examining the important B_s mixing constraint in section 2.1. In section 2.2, we define the mixed-up muon (MUM) and mixed-down muon (MDM) simplified models, followed by the more complete Third Family Hypercharge Model (TFHM). In section 3, we describe how we recast the ATLAS $Z' \to \mu^+\mu^-$ search and outline how other Run I and Run II measurements are checked against the model. Example parameter space points for each model are listed for illustration in section 4, before the combined collider constraints

JHEP08(2019)106

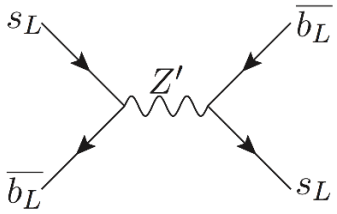

Figure 1. Feynman diagram of the tree-level Z' contribution to $B_s - \overline{B_s}$ mixing.

upon the models are presented. We summarise in section 5. In appendix A we define the fields. Properties of the three models studied throughout their parameter space are relegated to appendix B.

2 Models and constraints

We consider two representative models of Z's, following ref. [67], which introduced the naïve and the $33\mu\mu$ models. The tree-level Z' Lagrangian couplings that should be present in Z' models in order to explain the NCBAs are

$$\mathcal{L}_{Z'f} = \left(g_{sb}\overline{s_L}\not{Z}' b_L + \text{h.c.}\right) + g_{\mu\mu}\overline{\mu_L}\not{Z}'\mu_L + \ldots \tag{2.1}$$

A global fit to NCBAs and V_{ts} in ref. [25] found that the couplings and masses of Z' particles are constrained to be

$$g_{sb}g_{\mu\mu} = -x\left(\frac{M_{Z'}}{36\text{TeV}}\right)^2, \tag{2.2}$$

if g_{sb} and $g_{\mu\mu}$ are real, where $x = 1.06 \pm 0.16$ in the recent fit to the NCBAs from ref. [25]. Throughout this paper, we shall enforce eq. (2.2), typically taking the central value from the fit. In general, g_{sb} and $g_{\mu\mu}$ are complex. However, here, we take $g_{\mu\mu}$ to be real and positive and g_{sb} to be negative. In the models we introduce below, g_{sb} may have a small imaginary part. Since the full effects of complex phases are outside the scope of this work, whenever we refer to g_{sb} below, we shall implicitly refer to the real part of its value.

2.1 B_s mixing constraint

Z' models are subject to a number of constraints, a particularly strong one originating from measurements of $B_s - \overline{B_s}$ mixing, which constrains a function of g_{sb} and $M_{Z'}$. A Feynman diagram depicting the Z' contribution is shown in figure 1. The bound on a non-SM contribution depends upon the hadronic decay constant f_{B_s} and bag parameter B_s. The experimental measurement of the mixing parameter ΔM_s is [74] $\Delta M_s^{\text{exp}} = (17.757 \pm 0.021)\,\text{ps}^{-1}$. We use a determination of the SM prediction using recent lattice data and sum rules [75]

$$\Delta M_s^{\text{SM}} = (18.5^{+1.2}_{-1.5})\,\text{ps}^{-1}. \tag{2.3}$$

JHEP08(2019)106

In order to calculate the resulting bound on Z' models, we follow ref. [76]. In a model inducing the BSM operator

$$\mathcal{L}^{NP} = \frac{-4G_F}{\sqrt{2}}(V_{tb}V_{ts}^*)^2 \left[c_{sb}^{LL}(\overline{s_L}\gamma_\mu b_L)(\overline{s_L}\gamma^\mu b_L) + \text{H.c.}\right], \tag{2.4}$$

where $G_F = 1.1663787(6) \times 10^{-5}\,\text{GeV}^{-2}$ is the Fermi coupling constant, the SM prediction of B_s mixing is modified to $\Delta M_s^{\text{pred}} = |1 + c_{sb}^{LL}/R_{\text{SM}}^{\text{loop}}|\Delta M_S^{\text{SM}}$, where $R_{\text{SM}}^{\text{loop}} = 1.3397 \times 10^{-3}$. Our flavour changing Z's induce the Wilson coefficient

$$c_{sb}^{LL} = \frac{\eta^{LL}}{4\sqrt{2}G_F M_{Z'}^2}\frac{g_{sb}^2}{(V_{tb}V_{ts}^*)^2}, \tag{2.5}$$

η^{LL} takes renormalisation between $M_{Z'}$ and M_Z into account. It is a slow (logarithmic) function of $M_{Z'}$: $\eta^{LL} = 0.79$ for $M_{Z'} = 1\,\text{TeV}$, whereas $\eta^{LL} = 0.75$ for $M_{Z'} = 10\,\text{TeV}$ (we shall be concerned here with $M_{Z'} \leq 6\,\text{TeV}$). Here, we shall take $\eta^{LL} = 0.79$ whatever $M_{Z'}$, since this value gives the stronger limit out of the two numbers quoted and since η^{LL} is quite insensitive to $M_{Z'}$ anyway. Eq. (2.3) implies the 2σ lower bound $\Delta M_S^{\text{SM}} > 15.5\,\text{ps}^{-1}$, leaving room for a BSM contribution to make up a shortfall to the experimental 2σ upper bound if (by substituting $|V_{ts}^*V_{tb}| = 0.04$ into eq. (2.5))[1]

$$|g_{sb}| \lesssim M_{Z'}/(194\,\text{TeV}). \tag{2.6}$$

This places a strong constraint upon Z' models that explain the NCBAs [76].

2.2 Model definitions and couplings

Following ref. [62], we begin with simplified models originating from assuming that the Z' only couples to left-handed quarks and to left-handed leptons. Our direct search collider constraints are not strongly dependent upon the spin-structure of the Z' couplings and so this model should suffice to cover others (for example sharing the BSM operator between left-handed and right-handed muons). The Z' couplings to the mass eigenstate fermions in the model are

$$\mathcal{L} = \overline{\boldsymbol{u_L}}V\Lambda^{(Q)}V^\dagger \not{Z}'\boldsymbol{u}_L + \overline{\boldsymbol{d_L}}\Lambda^{(Q)}\not{Z}'\boldsymbol{d}_L + \overline{\boldsymbol{\nu_L}}U\Lambda^{(L)}U^\dagger \not{Z}'\boldsymbol{\nu}_L + \overline{\boldsymbol{e_L}}\Lambda^{(L)}\not{Z}'\boldsymbol{e}_L, \tag{2.7}$$

where we have written the Cabibbo-Kobayashi-Maskawa (CKM) matrix as V and the Pontecorvo-Maki-Nakagawa-Sakata matrix as U (see appendix 2.2 for field definitions). $\Lambda^{(Q)}$ and $\Lambda^{(L)}$ are 3 by 3 matrices of dimensionless couplings. In order to reproduce a Z' coupling to left-handed muons, as required to fit the B-anomalies, we use

$$\Lambda^{(L)} = g_{\mu\mu}\begin{pmatrix} 0 & 0 & 0 \\ 0 & 1 & 0 \\ 0 & 0 & 0 \end{pmatrix}. \tag{2.8}$$

The two simplified models introduced involve two different limiting assumptions for $\Lambda^{(Q)}$, in order to provide an estimate of how much the assumption changes predictions:

[1] This inferred bound has changed in recent years due to changes in data and lattice inputs: pre-2016, the denominator was 148 TeV [19], whereas from 2016–2019 the inferred denominator became 600 TeV [76].

JHEP08(2019)106

1. **The 'mixed-up-muon' (MUM) model**, with

$$\Lambda^{(Q)} = g_{sb} \begin{pmatrix} 0 & 0 & 0 \\ 0 & 0 & 1 \\ 0 & 1 & 0 \end{pmatrix}, \tag{2.9}$$

2. **The 'mixed-down-muon' (MDM) model**, with

$$\Lambda^{(Q)} = g_{tt} V^\dagger \cdot \begin{pmatrix} 0 & 0 & 0 \\ 0 & 0 & 0 \\ 0 & 0 & 1 \end{pmatrix} \cdot V \,. \tag{2.10}$$

Matching $\Lambda^{(Q)}$ here with eq. (2.1) identifies

$$g_{sb} = V_{ts}^* V_{tb} g_{tt}. \tag{2.11}$$

In the present article, we are not concerned with the effects of small complex phases: we shall take g_{tt} to be real.[2] $g_{tt} > 0$ ensures $g_{sb} < 0$ as required by eq. (2.2), since $V_{ts} \approx -0.04$ and $V_{tb} \approx 1$.

We may characterise the MUM and MDM simplified models by three important parameters: $M_{Z'}$, $|g_{sb}|$ and $g_{\mu\mu}$. In practice, we shall use $M_{Z'}$ and $|g_{sb}|$, whilst fixing $g_{\mu\mu}$ so as to fit the central values of the NCBAs in eq. (2.2). We note here that, since the MUM and MDM models are simplified, in reality the Z' might have more couplings than the ones introduced and so could be wider than predicted in the strict MUM or MDM limit. One could, instead of calculating the Z' width Γ, use the MUM or MDM limit as a lower bound and allow it to vary independently of g_{sb} and $g_{\mu\mu}$. We expect that increasing Γ will weaken search constraints, and so in some sense, neglecting this 'additional width' effect (which is the approach we shall take) is conservative.

The Third Family Hypercharge Model (TFHM) is based [61] on a $\mathrm{U}(1)_F$ gauge extension to the Standard Model, only the Higgs doublet, a new complex scalar SM singlet and third family fermions have non-zero $\mathrm{U}(1)_F$ quantum numbers. The heavy Z' comes from spontaneously breaking the $\mathrm{U}(1)_F$ and it is thus a more complete model than the MUM and MDM models. The model explains, in broad brush-strokes, the hierarchical heaviness of the third family of charged fermions and the smallness of CKM mixing angles. Anomaly cancellation implies that the $\mathrm{U}(1)_F$ quantum numbers of the third family fields are proportional to their hypercharges. The Z' couplings are, up to corrections $\mathcal{O}\left(M_Z^2/{M'_Z}^2\right)$

$$\begin{aligned} \mathcal{L}_{X\psi} = g_F \Bigg(& \frac{1}{6}\overline{\boldsymbol{u}_L}\Lambda^{(u_L)} \not{Z}' \boldsymbol{u}_L + \frac{1}{6}\overline{\boldsymbol{d}_L}\Lambda^{(d_L)} \not{Z}' \boldsymbol{d}_L - \frac{1}{2}\overline{\boldsymbol{\nu}_L}\Lambda^{(\nu_L)} \not{Z}' \boldsymbol{\nu}_L - \frac{1}{2}\overline{\boldsymbol{e}_L}\Lambda^{(e_L)} \not{Z}' \boldsymbol{e}_L \\ & + \frac{2}{3}\overline{\boldsymbol{u}_R}\Lambda^{(u_R)} \not{Z}' \boldsymbol{u}_R - \frac{1}{3}\overline{\boldsymbol{d}_R}\Lambda^{(d_R)} \not{Z}' \boldsymbol{d}_R - \overline{\boldsymbol{e}_R}\Lambda^{(e_R)} \not{Z}' \boldsymbol{e}_R \Bigg), \end{aligned} \tag{2.12}$$

[2] Although we include the effects of phases in the CKM matrix in our numerical simulations, they are not important for our results and we ignore them in analytic discussion.

JHEP08(2019)106

where we have defined the 3 by 3 dimensionless Hermitian coupling matrices

$$\Lambda^{(I)} \equiv V_I^\dagger \xi V_I, \tag{2.13}$$

$I \in \{u_L, d_L, e_L, \nu_L, u_R, d_R, e_R\}$ and

$$\xi = \begin{pmatrix} 0 & 0 & 0 \\ 0 & 0 & 0 \\ 0 & 0 & 1 \end{pmatrix}. \tag{2.14}$$

The V_I are unitary 3 by 3 matrices in family space and g_F is the dimensionless gauge coupling of $\mathrm{U}(1)_F$. For definiteness, we shall examine the phenomenological example case introduced in ref. [61]:

$$V_{d_L} = \begin{pmatrix} 1 & 0 & 0 \\ 0 & \cos\theta_{sb} & -\sin\theta_{sb} \\ 0 & \sin\theta_{sb} & \cos\theta_{sb} \end{pmatrix} \qquad \text{and} \qquad V_{e_L} = \begin{pmatrix} 1 & 0 & 0 \\ 0 & 0 & 1 \\ 0 & 1 & 0 \end{pmatrix}, \tag{2.15}$$

$V_{u_L} = V_{d_L} V^\dagger$, $V_{u_R} = V_{d_R} = V_{e_R} = 1$. To summarise, in the TFHM example case (TFHMeg), we have free parameters $|g_F|$, $M_{Z'}$ and θ_{sb}. In practice, we vary $M_{Z'}$ and θ_{sb}, setting g_F so as to satisfy the central value of the NCBAs, i.e. eq. (2.2), which translates to

$$g_F = \frac{M_{Z'}}{36\,\mathrm{TeV}} \sqrt{\frac{24x}{\sin(2\theta_{sb})}} \tag{2.16}$$

with $x = 1.06$.

3 Re-casting collider constraints

In its recent $Z' \to \mu^+\mu^-$ search, ATLAS defines [72] a fiducial cross-section σ where each muon has transverse momentum $p_T > 30\,\mathrm{GeV}$ and pseudo-rapidity $|\eta| < 2.5$. The di-muon invariant mass, $m_{\mu\mu} > 225\,\mathrm{GeV}$. No evidence for a significant bump in $m_{\mu\mu}$ was found, and so 95% upper limits on $\sigma \times BR(\mu^+\mu^-)$.

Re-casting constraints from such a bump-hunt in different Z' models is fairly simple: we must just calculate $\sigma \times BR(\mu^+\mu^-)$ for the model in question and apply the bound at the relevant value of $M_{Z'}$ and $\Gamma/M_{Z'}$. Efficiencies are taken into account in the experimental bound and so there is no need for us to perform a detector simulation. For generic $z \equiv \Gamma/M_{Z'}$, we interpolate/extrapolate the upper bound $s(z, M_{Z'})$ on $\sigma \times BR(\mu^+\mu^-)$ from those given by ATLAS at $z = 0$ and $z = 0.1$. In practice, we use a linear interpolation in $\ln s$:

$$s(z, M_{Z'}) = s(0, M_{Z'}) \left[\frac{s(0.1, M_{Z'})}{s(0, M_{Z'})}\right]^{\frac{z}{0.1}}. \tag{3.1}$$

Figure 2 shows examples of such a fit for five different values of $M_{Z'}$ compared to ATLAS upper limits. One point not lying on the line is due to a statistical fluctuation in data, but generally, the figure validates eq. (3.1) as being a reasonable fit within the range

JHEP08(2019)106

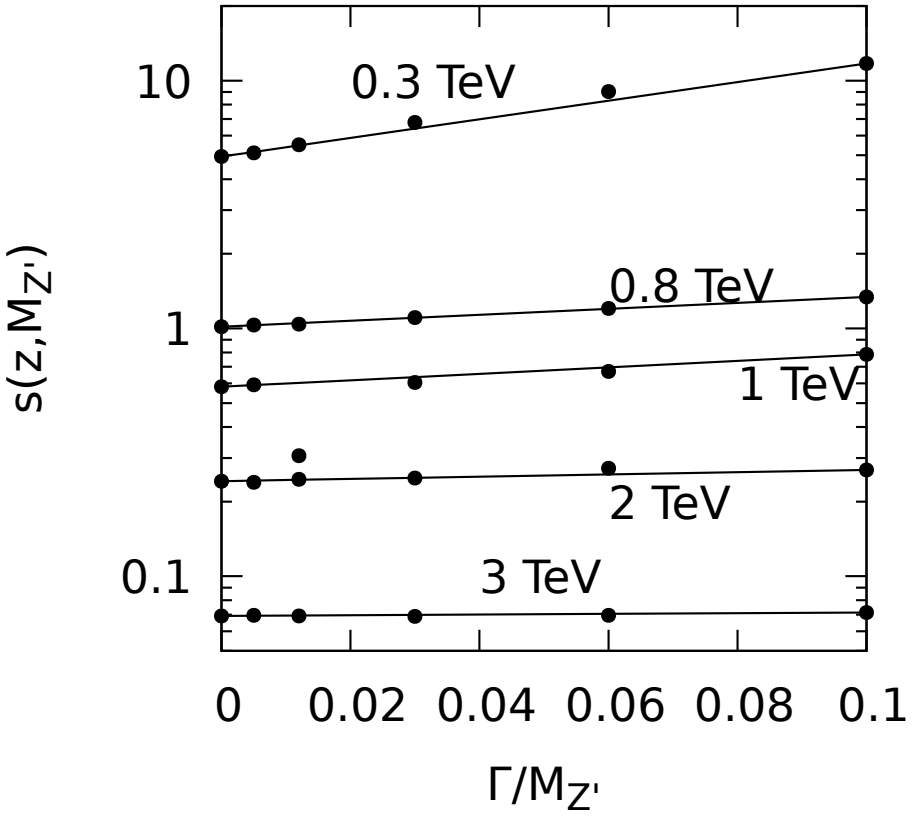

Figure 2. Examples of the fit in eq. (3.1) (shown by lines) compared to ATLAS data (shown by points), for various values of $M_{Z'}$, shown as a label by each line.

$\Gamma/M_{Z'} \in [0, 0.1]$. In general, we shall also use eq. (3.1) to extrapolate out of this range, however this will only turn out to play a rôle in part of the TFHMeg parameter space, which we shall delineate.

For the TFHMeg, we made a `UFO` file[3] by using `FeynRules` [77, 78]. The MUM model and MDM model files are taken from ref. [62]. These `UFO` files allow the `MadGraph` calculation of $\sigma \times BR(Z' \to \mu^+\mu^-)$ by `MadGraph_2_6_5` [79]. `MadGraph` estimates $\sigma \times BR(Z' \to \mu^+\mu^-)$ of the tree-level production processes shown in figure 3 in 13 TeV centre of mass energy pp collisions. We use 5-flavour parton distribution functions in order to re-sum the logarithms associated with the initial state b-quark [80].

3.1 Constraints from Contur

Introducing the BSM terms discussed above leads to other possible new processes and signatures in pp collisions in addition to the di-muon channel already considered. For example, in the TFHMeg model, the Z' has a branching fraction in the range 10–20% to $b\bar{b}$, up to 40% to $t\bar{t}$ and 20–30% to $\tau^+\tau^-$. It is often produced in association with additional b-jets, and the cross section for associated production with an isolated photon

[3]The `UFO` file is included in the Supplementary material information submitted with the `arXiv` version of this paper.

JHEP08(2019)106

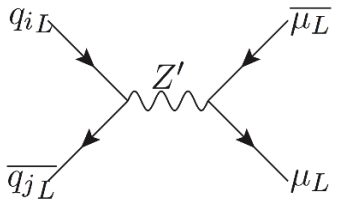

Figure 3. Feynman diagram of tree-level Z' production in the LHC, where $q_{i,j} \in \{u, c, d, s, b\}$ are such that the combination $q_{i\,L}\overline{q_{j\,L}}$ has zero electric charge.

can be as high as a few femtobarns. Many relevant measurements of such signatures have already been made by the LHC experiments, and we use the CONTUR [81] tool to check whether these measurements already disfavour any of the parameter space of our model. We use `Herwig7` [82, 83] and its `UFO` interface to calculate the cross section for all the new processes implied at the LHC by our models, and to inclusively generate the implied events. These events are then passed to Rivet [84] version 2.7, which contains an extensive library of particle-level collider measurements, especially from LHC Run I but also increasingly now from Run II. While these will not be as sensitive as individual searches using the full data set, they have the advantage of relative model-independence and ease of reinterpretation. All these measurements are in agreement with the SM, and CONTUR therefore treats them as SM background to a potential contribution from our models, evaluating whether the presence of an additional BSM contribution (in particular a Z' mass peak) would have been visible within the experimental uncertainty. This is then converted into an exclusion limit. Previous studies [81, 85, 86] have shown that this approach typically gives a comparable sensitivity to dedicated searches and can sometimes pick up unexpected additional signatures.

4 Results

In table 1, we display one point for each model studied, where the model parameters are chosen to fit the NCBAs and to be close to the exclusion of the ATLAS di-muon search in each case. We see that each point has a narrow Z': $\Gamma/M_{Z'} \leq 0.02$ (however, there are other points with larger values, as we shall see). In each model, the branching ratio into neutrinos is identical to that of muons and tagging an additional jet would result in a monojet $Z' \to$ invisible signature at the LHC. In the MUM model, we note the possible flavour changing channels $Z' \to t\bar{c} + \bar{c}t$, $Z' \to b\bar{s} + s\bar{b}$, which could also be used for searches. In the TFHMeg, decays to top pairs are 6 times more prevalent than those into muon pairs, which could prove to be an important channel for searches, as could decays into tau pairs (4 times more prevalent than muon pairs). Although these channels have a higher branching ratio than di-muons, the current bounds are sufficiently weaker such that di-muons (the only channel currently having been analysed for the full 139 fb^{-1} LHC Run II dataset) provide the strongest constraint. The table is instructive by exemplifying which PDFs are important for Z' production in each case. In the MDM model and the TFHMeg, $b\bar{b} \to Z'$ dominates, whereas in the MUM model, $b\bar{s} \to Z'$ dominates. The upper limit from

JHEP08(2019)106

MDM		MUM		TFHMeg	
parameter	value	parameter	value	parameter	value
M'_Z	1 TeV	$M_{Z'}$	0.8 TeV	$M_{Z'}$	1.9 TeV
g_{sb}	0.001	g_{sb}	0.01	θ_{sb}	0.08
$g_{\mu\mu}$	0.82	$g_{\mu\mu}$	0.052	g_F	0.67
quantity	value	quantity	value	quantity	value
$\Gamma/M_{Z'}$	0.018	$\Gamma/M_{Z'}$	8.4×10^{-5}	$\Gamma/M_{Z'}$	0.020
$BR(\mu^+\mu^-)$	0.50	$BR(\mu^+\mu^-)$	0.43	$BR(\mu^+\mu^-)$	0.07
$BR(t\bar{t})$	1.3×10^{-3}	$BR(t\bar{t})$	2.6×10^{-4}	$BR(t\bar{t})$	0.42
$BR(b\bar{b})$	1.3×10^{-3}	$BR(b\bar{s}+s\bar{b})$	0.09	$BR(b\bar{b})$	0.13
		$BR(t\bar{c}+c\bar{t})$	0.04	$BR(\tau^+\tau^-)$	0.30
channel	$\sigma\times BR$/fb	channel	$\sigma\times BR$/fb	channel	$\sigma\times BR$/fb
$b\bar{b}$	0.327			$b\bar{b}$	0.124
$\bar{s}b+\bar{b}s$	0.002	$\bar{s}b+\bar{b}s$	0.501	$\bar{s}b+\bar{b}s$	0.001
		$\bar{c}c$	0.002		
		$\bar{u}c+\bar{c}u$	0.001		
total	0.329	total	0.504	total	0.125
upper limit	1.07	upper limit	0.698	upper limit	0.241

Table 1. Illustration of example points in parameter space. The third parameter listed in each case is derived in terms of the two above it by the best fit to the NCBAs, i.e. eq. (2.2) with $x = 1.06$. 'channel' lists the contribution to the total Z' cross-section times branching ratio from the various quark parton distribution functions (PDFs). For each production mode, we list the Z' fiducial production cross-section times branching ratio into muon pairs $\sigma \times BR$. Other production modes have cross-sections that are smaller than 10^{-3} fb. The upper limit on the cross-section is the 95% CL_s bound derived from the ATLAS di-muon search [72] according to eq. (3.1).

the ATLAS di-muon search is shown for the particular $M_{Z'}$ of the parameter point, for the narrow width limit. In what follows, we include the dependence of these upper limits upon the width, as described in section 3.

Figure 4a displays the collider constraints on the MDM model. We see that the bounds from the ATLAS di-muon Z' search rule out a significant portion of parameter space that fits the central value of the NCBAs and is otherwise allowed. The shape of the various regions shown in figure 4a can be understood by looking at the properties of the model across parameter space, as shown in figure 6.

Since the Z' is produced through the quark coupling, the higher g_{sb}, the higher the Z' production cross-section, although it is suppressed by higher values of $M_{Z'}$ through the PDFs, as shown in figure 6c. Fitting the NCBAs means that $g_{\mu\mu}$ is small at small $M_{Z'}$ and large $|g_{sb}|$, as displayed by figure 6d. This region has small $BR(Z' \to \mu^+\mu^-)$, as figure 6b shows, which limits the exclusion of the ATLAS di-muon search in the top left-hand corner

JHEP08(2019)106

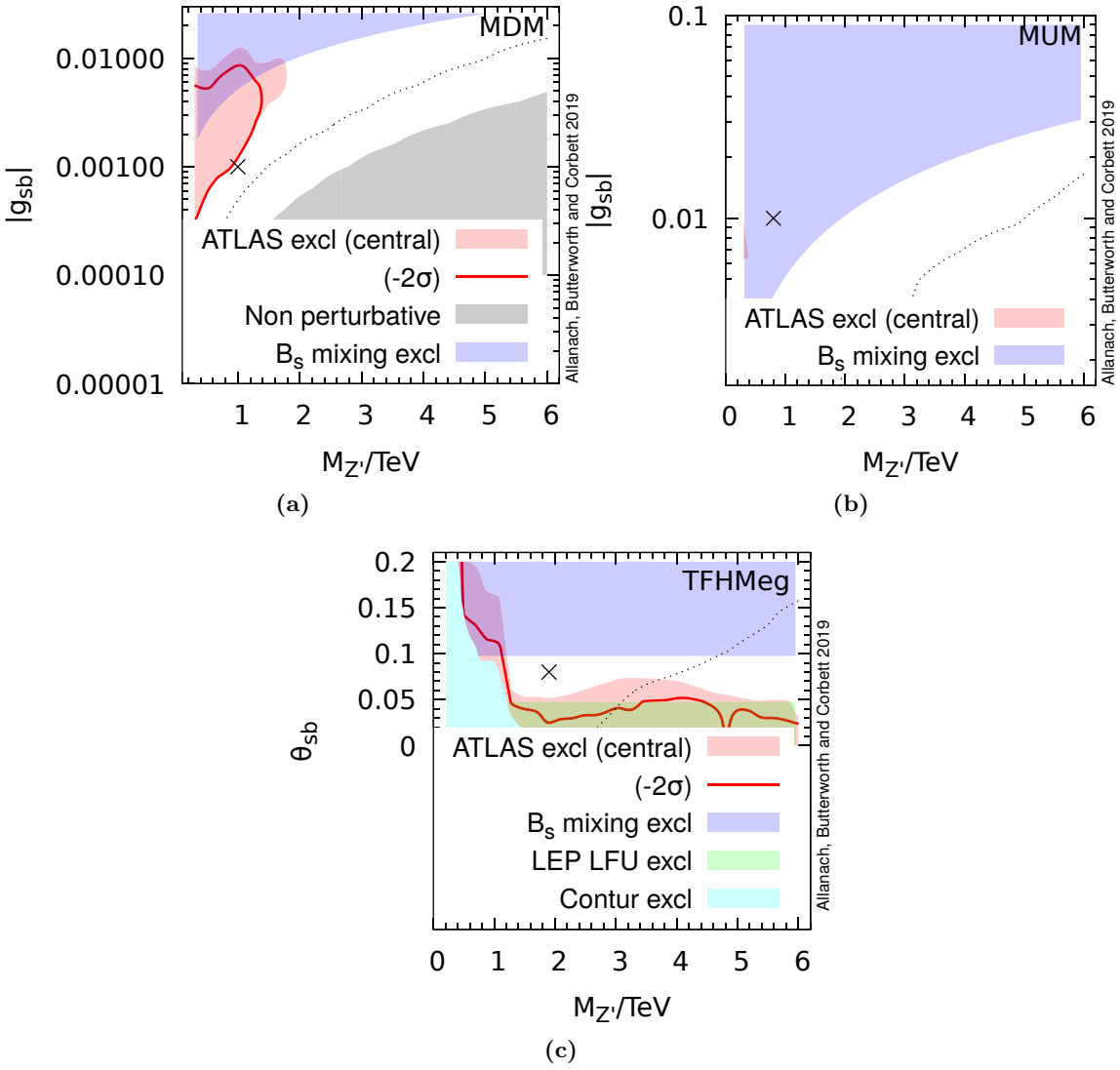

Figure 4. Collider constraints on the central fits of the models to NCBAs for (a) the MDM model, (b) the MUM model and (c) the TFHMeg. The allowed region is shown in white. Everywhere throughout the parameter plane shown, the third parameter is fixed by the central fit to the NCBAs: $g_{\mu\mu}$ as in eq. (2.2) in (a) and (b), and g_F as in eq. (2.16) in (c), each with $x = 1.06$. The region marked 'non-perturbative' in (a) has $\Gamma_{Z'}/M_{Z'} > 1$, whereas the dotted lines display where $\Gamma_{Z'}/M_{Z'} = 0.1$ for each model (this quantity increases toward the right-hand side of each plot). The B_s mixing constraint from eq. (2.6) excludes the 'B_s mixing excl' region. In (c), the region excluded by the LEP lepton flavour universality is shown by the legend as 'LEP LFU excl' and is calculated in ref. [61]. The ATLAS 139 fb^{-1} di-muon Z' exclusion region is marked 'ATLAS excl (central)' in each plot. Varying the NCBA fit to be 2σ toward the SM limit results in the smaller '(-2σ)' exclusion region. The dark crosses show the locations of the example points listed in table 1. In (c), we also display the region excluded by CONTUR at the 95% CL_s level.

JHEP08(2019)106

of figure 4a. Conversely, the region with large $M_{Z'}$ and small $|g_{sb}|$ requires such a large value of $g_{\mu\mu}$ that the model becomes non-perturbative (where the Z' width is equal to or larger than the mass), and we could not trust our results there. Fortunately, this does not impact any of the bounds we have derived.

Constraints on the MUM model are summarised in figure 4b. We see here that the B_s mixing constraint already covers all of the region which the ATLAS di-muon search excludes (which is hardly visible in the plot), in contrast to the MDM model shown in figure 4a. The production processes do not benefit from the large $b\bar{b}$ contribution present in the MDM model, as table 1 illustrates. This is essentially because the MDM model has a $Z'\bar{b}b$ coupling $\propto g_{sb}/|V_{ts}|$ i.e. enhanced by $1/|V_{ts}| \sim 25$. We may understand the shape of the ATLAS constraint by referring to figure 7 in appendix B: the branching ratio into muons increases for smaller $|g_{sb}|$ and larger $M_{Z'}$, which competes with the cross-section which increases toward the top left-hand corner of figure 4b. Everywhere that the ATLAS di-muon constraints are active, the Z' is narrow.

Combined constraints on the TFHMeg are shown in figure 4c. We see that the ATLAS di-muon search has a strong effect on the parameter space when combined with the B_s mixing constraint: $M_{Z'} > 1.2\,\text{TeV}$, for a central fit to the NCBAs. The region excluded by LEP flavour universality was calculated in ref. [61], and occurs because the Z picks up small differences in its couplings to electrons as compared to muons due to $Z - Z'$ mixing. The model is non-perturbative for $M_{Z'} \geq 8.4\,\text{TeV}$ [61]. The white region is a relatively small portion of parameter space, but really one should take the weaker limits at '(-2σ)', given the possibility of statistical variations of the fit to the NCBAs. The region to the right-hand side of the dotted line has $\Gamma/M_{Z'} > 0.1$, and so involves an extrapolation of the fit to data given in eq. (3.1) for this region (rather than an interpolation).

Contur exclusion limits are displayed at the left-hand side of the figure and the excluded region is marked 'Contur excl'. There are *no* such exclusion limits in the parameter region shown for MDM or MUM, as the detailed Contur plots in figure 5 show. The Contur constraints show 'due diligence', in that the interesting parameter space is not yet ruled out by a large number of LHC SM measurements. Even though some measurements do receive BSM contributions to the fiducial cross section (for example the ATLAS 13 TeV $t\bar{t}b\bar{b}$ [87] and 8 TeV di-lepton-plus-di-jet measurements [88], and the CMS 13 TeV $t\bar{t}$ measurement [89]), the measurement precision is not yet sufficient to have a strong exclusion impact. Such exclusion as there is comes mainly from the ATLAS 8 TeV high-mass Drell-Yan measurement [90], and thus does not have the reach of the 13 TeV full Run II search.

5 Summary

Our focal results are the combined dominant constraints on Z' models (the MUM model, the MDM model and the TFHMeg) which fit the NBCAs and are shown in figure 4. The B_s mixing constraint is important, as well as a recent ATLAS $Z'\mu^+\mu^-$ search, performed on $139\,\text{fb}^{-1}$ of 13 TeV pp LHC collisions. The ATLAS search is probing the otherwise allowed parameter space of the MDM simplified model, and we may expect the TeV HL-LHC to

JHEP08(2019)106

Channel	$\mu^+\mu^-$	$t\bar{t}$	$\tau^+\tau^-$	$b\bar{b}$	$\bar{\nu}_i\nu_j$
$\sigma \times BR$/fb	0.010	0.056	0.04	0.017	0.010

Table 2. HL-LHC ($\sqrt{s} = 14\,\text{TeV}$) minimum fiducial cross section times branching ratios for different final-state channels in the TFHMeg.

increase coverage of the parameter space [62, 67]. On the other hand, the MUM simplified model is currently more constrained by the B_s mixing constraint, and likely will require an increase in energy [62, 67] (for example to HE-LHC [91] or FCC, [68]) for di-muon searches to probe the remaining parameter space. The B_s mixing constraint is particularly constraining, but there has been significant movement on it in the last four years, mainly due to different estimates of the SM contribution. The 95% CL bound has been $M_{Z'}/g_{sb} > 148, 600, 194\,\text{TeV}$, respectively. We might therefore expect further movement upon the bound in the future, and this could have a large impact on the constraints. Taking the current bound of 194 TeV at face value, we extract (from the '(-2σ)' bounds in figure 4c and from figure 8b) that $\sigma \times BR(Z' \to \mu^+\mu^-) \geq 2.6 \times 10^{-3}\,\text{fb}$ in the TFHMeg at a centre of mass energy $\sqrt{s} = 13\,\text{TeV}$. The lower bound is saturated for $M_{Z'} = 3.5\,\text{TeV}$, $\theta_{sb} = 0.1$. At $\sqrt{s} = 14\,\text{TeV}$, we estimate (from this point) the minimum cross-sections in table 2. Since the nominal integrated luminosity for the HL-LHC is $\mathcal{L} = 3000\,\text{fb}^{-1}$, we may expect at least $S = 30$ signal $Z' \to \mu^+\mu^-$ events. We are therefore hopeful of the TFHMeg HL-LHC Z' search prospects.[4]

Acknowledgments

This work has been partially supported by STFC consolidated grants ST/P000681/1 and ST/N000285/1. BCA and JMB thank the *(Re)interpreting the results of new physics searches at the LHC* workshop, where part of this work was carried out. BCA thanks A Lenz and the Cambridge SUSY Working Group for discussions. This work has received funding from the European Union's Horizon 2020 research and innovation programme as part of the Marie Skłodowska-Curie Innovative Training Network MCnetITN3 (grant agreement no. 722104).

A Field definitions

We use the following field definitions in terms of representations of $\text{SU}(3) \times \text{SU}(2)_L \times \text{U}(1)_Y$: $\boldsymbol{Q}_L = (3,\ 2,\ +1/6) = (\boldsymbol{u}_L, \boldsymbol{d}_L)^T$, $\boldsymbol{L}_L = (1,\ 2,\ -1/2) = (\boldsymbol{\nu}_L, \boldsymbol{e}_L)^T$, $Z' = (1\,,1\,,0)$, where bold face denotes a 3-dimensional vector in family space. These fields are implicitly written in the mass eigenbasis.

[4] Background estimates, which are beyond the scope of this work, would be required to properly calculate the sensitivity.

JHEP08(2019)106

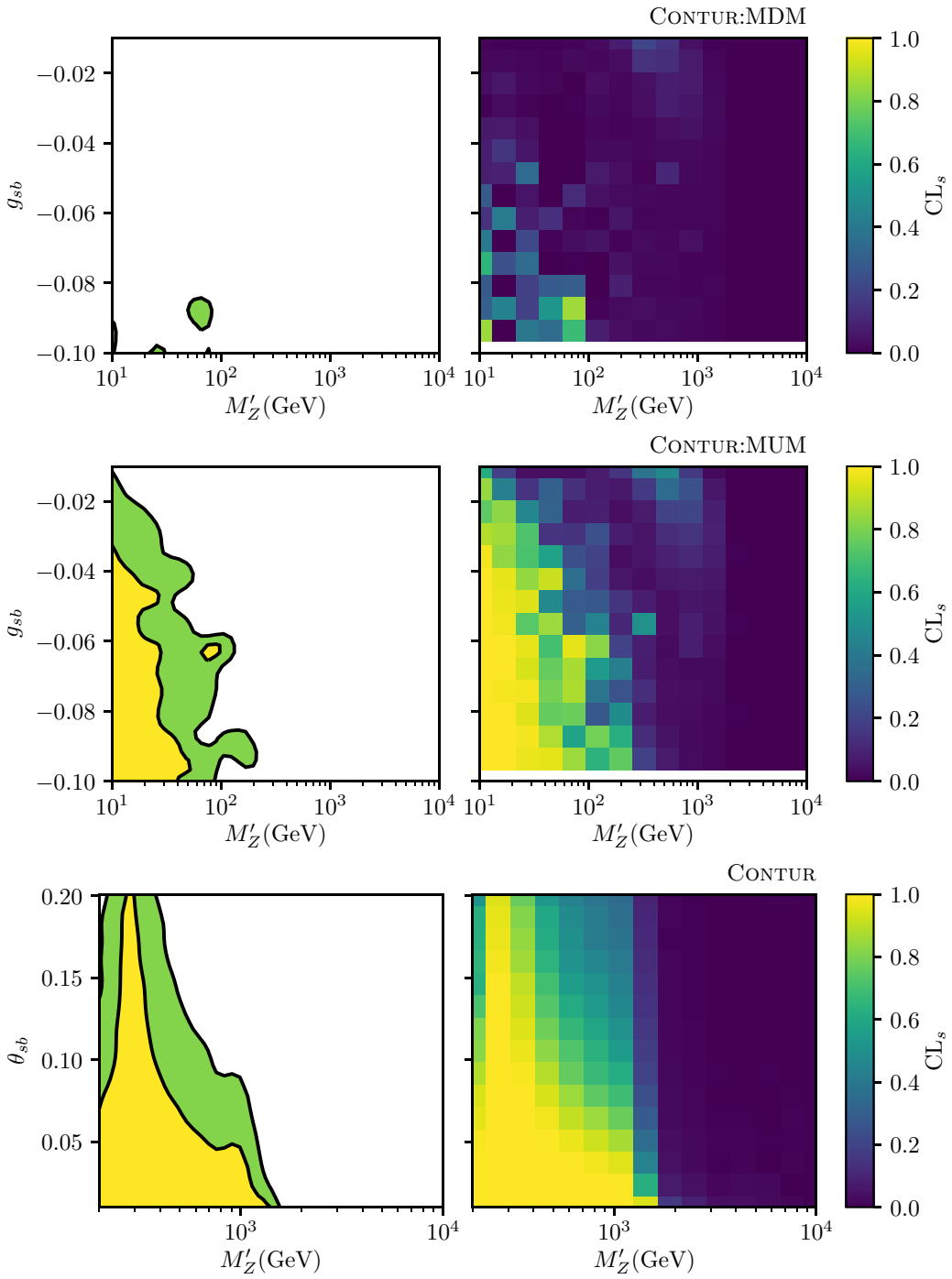

Figure 5. CONTUR constraints on the MDM model (top), the MUM model (middle) and the TFHMeg (bottom). In the left-hand panels, we show regions excluded at the 68% and 95% CL_s levels. In the right-hand panels, we show the CL_s values, where 95% excluded values are > 0.95. Everywhere throughout the parameter plane shown, the NCBAs are fit by fixing $g_{\mu\mu}$ and g_F as in eqs. (2.2), 2.16, respectively, for $x = 1.06$.

JHEP08(2019)106

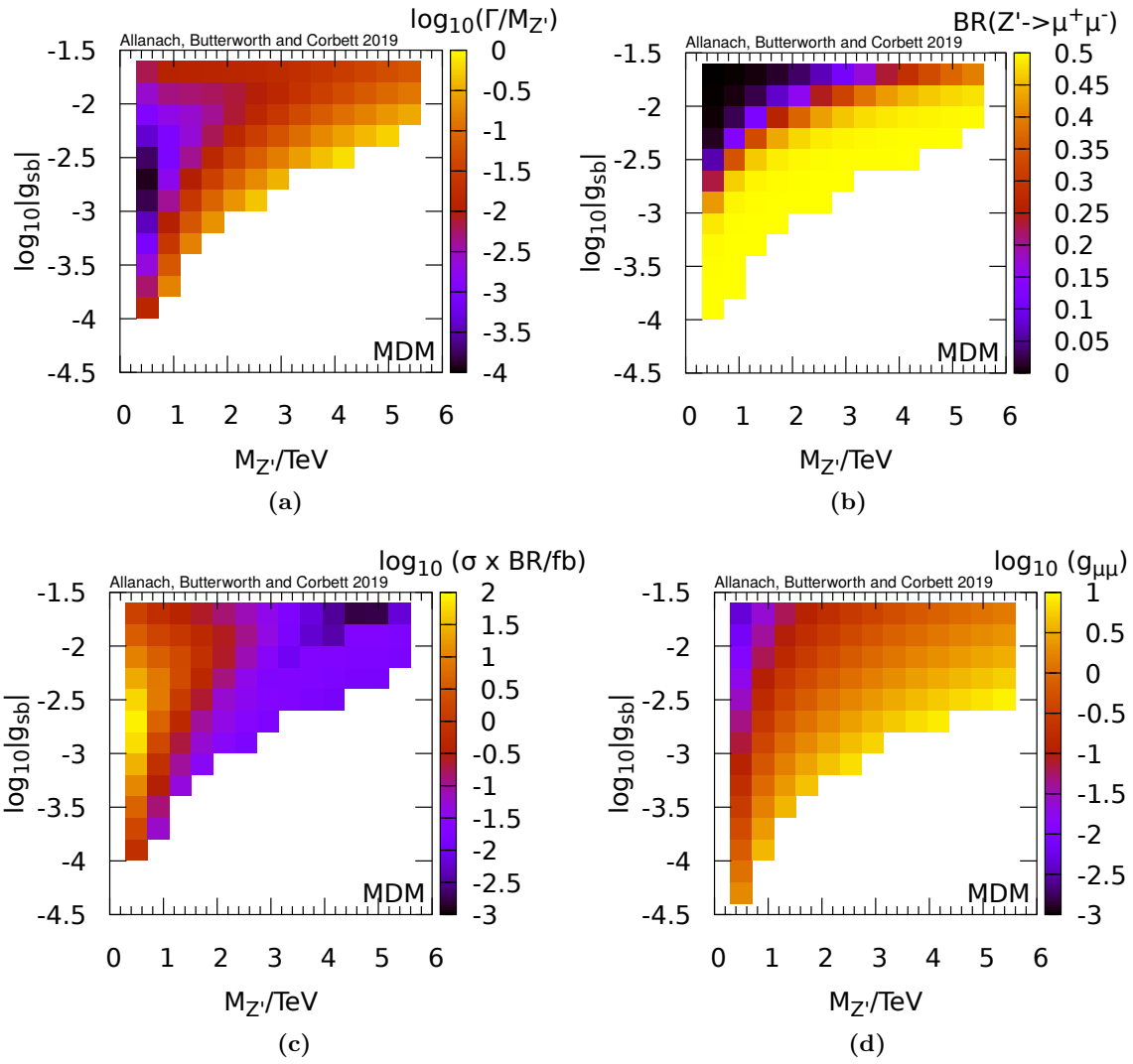

Figure 6. Properties of the central fit of the MDM model to NCBAs. In (a), we show the Z' width divided by its mass, $\Gamma/M_{Z'}$. In (b), the branching ratio into di-muons is shown, in (c) the fiducial Z' production cross section multiplied by its branching ratio into di-muons is displayed. (d) shows $g_{\mu\mu}$ coming from the central fit to NCBAs. The white region is non-perturbative.

JHEP08(2019)106

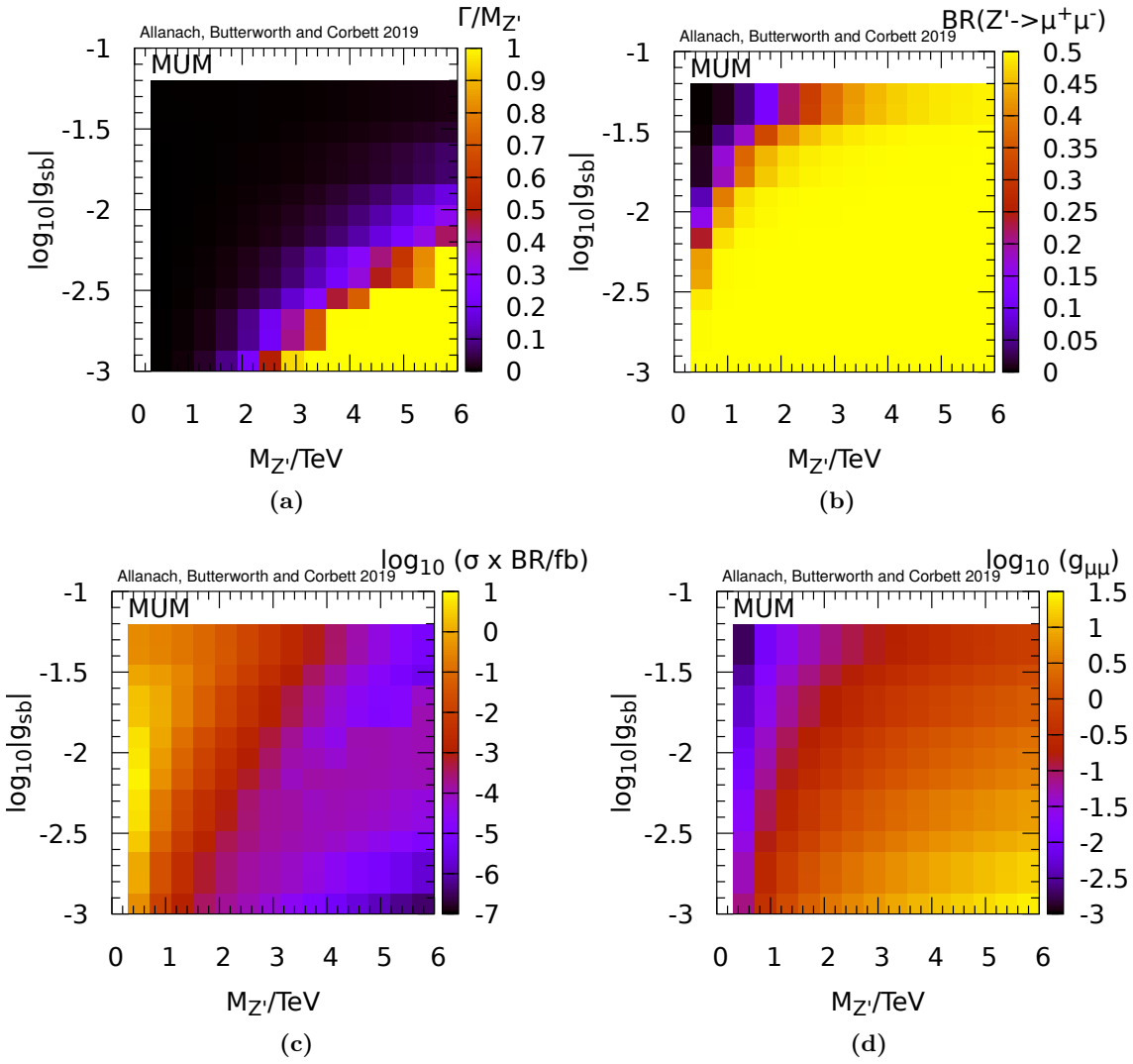

Figure 7. Properties of the central fit of the MUM model to NCBAs. In (a), we show the Z' width divided by its mass, $\Gamma/M_{Z'}$. In (b), the branching ratio into di-muons is shown, in (c) the fiducial Z' production cross section multiplied by its branching ratio into di-muons is displayed. (d) shows $g_{\mu\mu}$ coming from the central fit to NCBAs.

JHEP08(2019)106

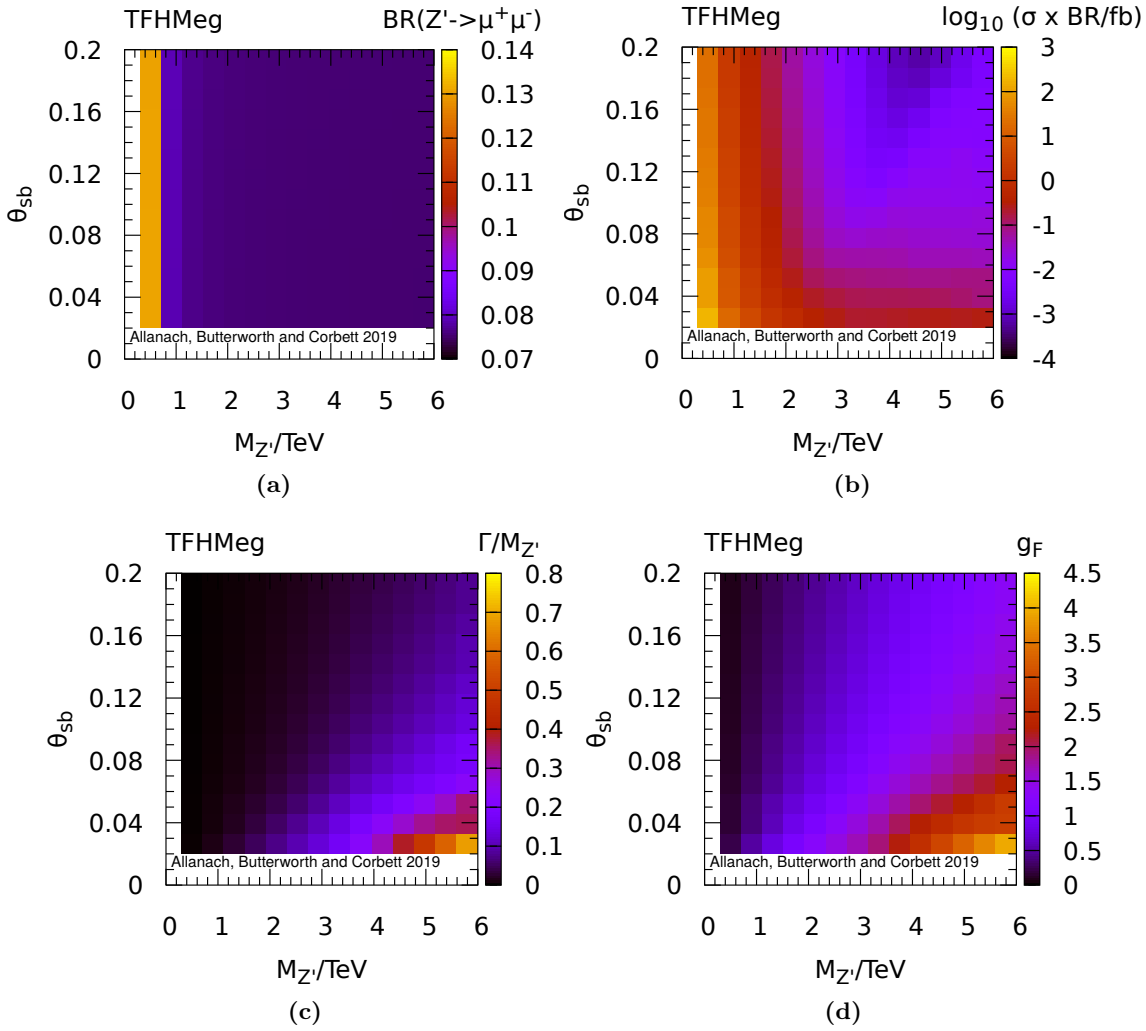

Figure 8. Properties of the TFHMeg. Everywhere throughout the parameter plane shown, the NCBAs are fit by fixing g_F as in eq. (2.16) for $x = 1.06$ and shown in panel (d).

B Properties of the models

We display the CONTUR constraints on the different models in figure 5. There are essentially no constraints upon the MDM model, whereas the MUM model is somewhat constrained for $M_{Z'} < 100\,\text{GeV}$. The strongest constraints are upon the TFHMeg, which extend to $M_{Z'} = 1.5\,\text{TeV}$, for low θ_{sb} (where g_F is high).

We display some properties of the MDM model across parameter space in figure 6, some of the MUM model in figure 7 and some of the TFHMeg in figure 8.

JHEP08(2019)106

References

[1] LHCb collaboration, *Test of lepton universality with $B^0 \to K^{*0}\ell^+\ell^-$ decays*, *JHEP* **08** (2017) 055 [arXiv:1705.05802] [INSPIRE].

[2] LHCb collaboration, *Search for lepton-universality violation in $B^+ \to K^+\ell^+\ell^-$ decays*, *Phys. Rev. Lett.* **122** (2019) 191801 [arXiv:1903.09252] [CERN-EP-2019-043] [LHCB-PAPER-2019-009] [INSPIRE].

[3] ATLAS collaboration, *Study of the rare decays of B_s^0 and B^0 mesons into muon pairs using data collected during 2015 and 2016 with the ATLAS detector*, *JHEP* **04** (2019) 098 [arXiv:1812.03017] [INSPIRE].

[4] CMS collaboration, *Measurement of the $B_s^0 \to \mu^+\mu^-$ Branching Fraction and Search for $B^0 \to \mu^+\mu^-$ with the CMS Experiment*, *Phys. Rev. Lett.* **111** (2013) 101804 [arXiv:1307.5025] [INSPIRE].

[5] CMS and LHCb collaborations, *Observation of the rare $B_s^0 \to \mu^+\mu^-$ decay from the combined analysis of CMS and LHCb data*, *Nature* **522** (2015) 68 [arXiv:1411.4413] [INSPIRE].

[6] LHCb collaboration, *Measurement of the $B_s^0 \to \mu^+\mu^-$ branching fraction and effective lifetime and search for $B^0 \to \mu^+\mu^-$ decays*, *Phys. Rev. Lett.* **118** (2017) 191801 [arXiv:1703.05747] [INSPIRE].

[7] LHCb collaboration, *Measurement of Form-Factor-Independent Observables in the Decay $B^0 \to K^{*0}\mu^+\mu^-$*, *Phys. Rev. Lett.* **111** (2013) 191801 [arXiv:1308.1707] [INSPIRE].

[8] LHCb collaboration, *Angular analysis of the $B^0 \to K^{*0}\mu^+\mu^-$ decay using $3\,fb^{-1}$ of integrated luminosity*, *JHEP* **02** (2016) 104 [arXiv:1512.04442] [INSPIRE].

[9] ATLAS collaboration, *Angular analysis of $B_d^0 \to K^*\mu^+\mu^-$ decays in pp collisions at $\sqrt{s} = 8$ TeV with the ATLAS detector*, ATLAS-CONF-2017-023 (2017) [INSPIRE].

[10] CMS collaboration, *Measurement of the P_1 and P_5' angular parameters of the decay $B^0 \to K^{*0}\mu^+\mu^-$ in proton-proton collisions at $\sqrt{s} = 8$ TeV*, CMS-PAS-BPH-15-008 (2017) [INSPIRE].

[11] CMS collaboration, *Angular analysis of the decay $B^0 \to K^{*0}\mu^+\mu^-$ from pp collisions at $\sqrt{s} = 8$ TeV*, *Phys. Lett.* **B 753** (2016) 424 [arXiv:1507.08126] [INSPIRE].

[12] C. Bobeth, M. Chrzaszcz, D. van Dyk and J. Virto, *Long-distance effects in $B \to K^*\ell\ell$ from analyticity*, *Eur. Phys. J.* **C 78** (2018) 451 [arXiv:1707.07305] [INSPIRE].

[13] W. Altmannshofer and D.M. Straub, *New Physics in $B \to K^*\mu\mu$?*, *Eur. Phys. J.* **C 73** (2013) 2646 [arXiv:1308.1501] [INSPIRE].

[14] W. Altmannshofer and D.M. Straub, *New physics in $b \to s$ transitions after LHC run 1*, *Eur. Phys. J.* **C 75** (2015) 382 [arXiv:1411.3161] [INSPIRE].

[15] W. Altmannshofer, P. Stangl and D.M. Straub, *Interpreting Hints for Lepton Flavor Universality Violation*, *Phys. Rev.* **D 96** (2017) 055008 [arXiv:1704.05435] [INSPIRE].

[16] M. Ciuchini et al., *On Flavourful Easter eggs for New Physics hunger and Lepton Flavour Universality violation*, *Eur. Phys. J.* **C 77** (2017) 688 [arXiv:1704.05447] [INSPIRE].

[17] B. Capdevila, A. Crivellin, S. Descotes-Genon, J. Matias and J. Virto, *Patterns of New Physics in $b \to s\ell^+\ell^-$ transitions in the light of recent data*, *JHEP* **01** (2018) 093 [arXiv:1704.05340] [INSPIRE].

JHEP08(2019)106

[18] L.-S. Geng, B. Grinstein, S. Jäger, J. Martin Camalich, X.-L. Ren and R.-X. Shi, *Towards the discovery of new physics with lepton-universality ratios of $b \to s\ell\ell$ decays*, *Phys. Rev.* **D 96** (2017) 093006 [arXiv:1704.05446] [INSPIRE].

[19] G. D'Amico et al., *Flavour anomalies after the R_{K^*} measurement*, *JHEP* **09** (2017) 010 [arXiv:1704.05438] [INSPIRE].

[20] S. Di Chiara et al., *Minimal flavor-changing Z' models and muon $g-2$ after the R_{K^*} measurement*, *Nucl. Phys.* **B 923** (2017) 245 [arXiv:1704.06200] [INSPIRE].

[21] J. Albrecht, F. Bernlochner, M. Kenzie, S. Reichert, D. Straub and A. Tully, *Future prospects for exploring present day anomalies in flavour physics measurements with Belle II and LHCb*, arXiv:1709.10308 [INSPIRE].

[22] M. Algueró et al., *Emerging patterns of New Physics with and without Lepton Flavour Universal contributions*, arXiv:1903.09578 [INSPIRE].

[23] A.K. Alok, A. Dighe, S. Gangal and D. Kumar, *Continuing search for new physics in $b \to s\mu\mu$ decays: two operators at a time*, *JHEP* **06** (2019) 089 [arXiv:1903.09617] [INSPIRE].

[24] M. Ciuchini et al., *New Physics in $b \to s\ell^+\ell^-$ confronts new data on Lepton Universality*, arXiv:1903.09632 [INSPIRE].

[25] J. Aebischer, W. Altmannshofer, D. Guadagnoli, M. Reboud, P. Stangl and D.M. Straub, *B-decay discrepancies after Moriond 2019*, arXiv:1903.10434 [INSPIRE].

[26] K. Kowalska, D. Kumar and E.M. Sessolo, *Implications for New Physics in $b \to s\mu\mu$ transitions after recent measurements by Belle and LHCb*, arXiv:1903.10932 [INSPIRE].

[27] A. Arbey, T. Hurth, F. Mahmoudi, D.M. Santos and S. Neshatpour, *Update on the $b \to s$ anomalies*, arXiv:1904.08399 [INSPIRE].

[28] J. Ellis, M. Fairbairn and P. Tunney, *Anomaly-Free Models for Flavour Anomalies*, *Eur. Phys. J.* **C 78** (2018) 238 [arXiv:1705.03447] [INSPIRE].

[29] B.C. Allanach, J. Davighi and S. Melville, *An Anomaly-free ATLAS: charting the space of flavour-dependent gauged* U(1) *extensions of the Standard Model*, *JHEP* **02** (2019) 082 [arXiv:1812.04602] [INSPIRE].

[30] R. Gauld, F. Goertz and U. Haisch, *On minimal Z' explanations of the $B \to K^*\mu^+\mu^-$ anomaly*, *Phys. Rev.* **D 89** (2014) 015005 [arXiv:1308.1959] [INSPIRE].

[31] A.J. Buras, F. De Fazio and J. Girrbach, *331 models facing new $b \to s\mu^+\mu^-$ data*, *JHEP* **02** (2014) 112 [arXiv:1311.6729] [INSPIRE].

[32] A.J. Buras and J. Girrbach, *Left-handed Z' and Z FCNC quark couplings facing new $b \to s\mu^+\mu^-$ data*, *JHEP* **12** (2013) 009 [arXiv:1309.2466] [INSPIRE].

[33] W. Altmannshofer, S. Gori, M. Pospelov and I. Yavin, *Quark flavor transitions in $L_\mu - L_\tau$ models*, *Phys. Rev.* **D 89** (2014) 095033 [arXiv:1403.1269] [INSPIRE].

[34] A.J. Buras, F. De Fazio and J. Girrbach-Noe, *Z–Z' mixing and Z-mediated FCNCs in $\mathrm{SU}(3)_C \times \mathrm{SU}(3)_L \times \mathrm{U}(1)_X$ models*, *JHEP* **08** (2014) 039 [arXiv:1405.3850] [INSPIRE].

[35] A. Crivellin, G. D'Ambrosio and J. Heeck, *Explaining $h \to \mu^\pm\tau^\mp$, $B \to K^*\mu^+\mu^-$ and $B \to K\mu^+\mu^-/B \to Ke^+e^-$ in a two-Higgs-doublet model with gauged $L_\mu - L_\tau$*, *Phys. Rev. Lett.* **114** (2015) 151801 [arXiv:1501.00993] [INSPIRE].

[36] A. Crivellin, G. D'Ambrosio and J. Heeck, *Addressing the LHC flavor anomalies with horizontal gauge symmetries*, *Phys. Rev.* **D 91** (2015) 075006 [arXiv:1503.03477] [INSPIRE].

JHEP08(2019)106

[37] D. Aristizabal Sierra, F. Staub and A. Vicente, *Shedding light on the $b \to s$ anomalies with a dark sector*, *Phys. Rev.* **D 92** (2015) 015001 [arXiv:1503.06077] [INSPIRE].

[38] A. Crivellin, L. Hofer, J. Matias, U. Nierste, S. Pokorski and J. Rosiek, *Lepton-flavour violating B decays in generic Z' models*, *Phys. Rev.* **D 92** (2015) 054013 [arXiv:1504.07928] [INSPIRE].

[39] A. Celis, J. Fuentes-Martin, M. Jung and H. Serodio, *Family nonuniversal Z' models with protected flavor-changing interactions*, *Phys. Rev.* **D 92** (2015) 015007 [arXiv:1505.03079] [INSPIRE].

[40] A. Greljo, G. Isidori and D. Marzocca, *On the breaking of Lepton Flavor Universality in B decays*, *JHEP* **07** (2015) 142 [arXiv:1506.01705] [INSPIRE].

[41] W. Altmannshofer and I. Yavin, *Predictions for lepton flavor universality violation in rare B decays in models with gauged $L_\mu - L_\tau$*, *Phys. Rev.* **D 92** (2015) 075022 [arXiv:1508.07009] [INSPIRE].

[42] B. Allanach, F.S. Queiroz, A. Strumia and S. Sun, *Z' models for the LHCb and $g-2$ muon anomalies*, *Phys. Rev.* **D 93** (2016) 055045 [*Erratum ibid.* **D 95** (2017) 119902] [arXiv:1511.07447] [INSPIRE].

[43] A. Falkowski, M. Nardecchia and R. Ziegler, *Lepton Flavor Non-Universality in B-meson Decays from a* U(2) *Flavor Model*, *JHEP* **11** (2015) 173 [arXiv:1509.01249] [INSPIRE].

[44] C.-W. Chiang, X.-G. He and G. Valencia, *Z' model for $b \to s\ell\bar{\ell}$ flavor anomalies*, *Phys. Rev.* **D 93** (2016) 074003 [arXiv:1601.07328] [INSPIRE].

[45] D. Bečirević, O. Sumensari and R. Zukanovich Funchal, *Lepton flavor violation in exclusive $b \to s$ decays*, *Eur. Phys. J.* **C 76** (2016) 134 [arXiv:1602.00881] [INSPIRE].

[46] S.M. Boucenna, A. Celis, J. Fuentes-Martin, A. Vicente and J. Virto, *Non-abelian gauge extensions for B-decay anomalies*, *Phys. Lett.* **B 760** (2016) 214 [arXiv:1604.03088] [INSPIRE].

[47] S.M. Boucenna, A. Celis, J. Fuentes-Martin, A. Vicente and J. Virto, *Phenomenology of an* SU(2) × SU(2) × U(1) *model with lepton-flavour non-universality*, *JHEP* **12** (2016) 059 [arXiv:1608.01349] [INSPIRE].

[48] P. Ko, Y. Omura, Y. Shigekami and C. Yu, *LHCb anomaly and B physics in flavored Z' models with flavored Higgs doublets*, *Phys. Rev.* **D 95** (2017) 115040 [arXiv:1702.08666] [INSPIRE].

[49] R. Alonso, P. Cox, C. Han and T.T. Yanagida, *Anomaly-free local horizontal symmetry and anomaly-full rare B-decays*, *Phys. Rev.* **D 96** (2017) 071701 [arXiv:1704.08158] [INSPIRE].

[50] R. Alonso, P. Cox, C. Han and T.T. Yanagida, *Flavoured $B-L$ local symmetry and anomalous rare B decays*, *Phys. Lett.* **B 774** (2017) 643 [arXiv:1705.03858] [INSPIRE].

[51] Y. Tang and Y.-L. Wu, *Flavor non-universal gauge interactions and anomalies in B-meson decays*, *Chin. Phys.* **C 42** (2018) 033104 [arXiv:1705.05643] [INSPIRE].

[52] C. Bonilla, T. Modak, R. Srivastava and J.W.F. Valle, $\mathrm{U}(1)_{B_3-3L_\mu}$ *gauge symmetry as a simple description of $b \to s$ anomalies*, *Phys. Rev.* **D 98** (2018) 095002 [arXiv:1705.00915] [INSPIRE].

[53] D. Bhatia, S. Chakraborty and A. Dighe, *Neutrino mixing and R_K anomaly in* $\mathrm{U}(1)_X$ *models: a bottom-up approach*, *JHEP* **03** (2017) 117 [arXiv:1701.05825] [INSPIRE].

JHEP08(2019)106

[54] C.-H. Chen and T. Nomura, *Penguin $b \to s\ell'^{+}\ell'^{-}$ and B-meson anomalies in a gauged $L_\mu - L_\tau$*, *Phys. Lett.* **B 777** (2018) 420 [arXiv:1707.03249] [INSPIRE].

[55] G. Faisel and J. Tandean, *Connecting $b \to s\ell\bar{\ell}$ anomalies to enhanced rare nonleptonic $\overline{B}{}^0_s$ decays in Z' model*, *JHEP* **02** (2018) 074 [arXiv:1710.11102] [INSPIRE].

[56] K. Fuyuto, H.-L. Li and J.-H. Yu, *Implications of hidden gauged* U(1) *model for B anomalies*, *Phys. Rev.* **D 97** (2018) 115003 [arXiv:1712.06736] [INSPIRE].

[57] L. Bian, H.M. Lee and C.B. Park, *B-meson anomalies and Higgs physics in flavored* U(1)′ *model*, *Eur. Phys. J.* **C 78** (2018) 306 [arXiv:1711.08930] [INSPIRE].

[58] M. Abdullah et al., *Bottom-quark fusion processes at the LHC for probing Z' models and B-meson decay anomalies*, *Phys. Rev.* **D 97** (2018) 075035 [arXiv:1707.07016] [INSPIRE].

[59] S.F. King, *$R_{K^{(*)}}$ and the origin of Yukawa couplings*, *JHEP* **09** (2018) 069 [arXiv:1806.06780] [INSPIRE].

[60] G.H. Duan, X. Fan, M. Frank, C. Han and J.M. Yang, *A minimal* U(1)′ *extension of MSSM in light of the B decay anomaly*, *Phys. Lett.* **B 789** (2019) 54 [arXiv:1808.04116] [INSPIRE].

[61] B.C. Allanach and J. Davighi, *Third family hypercharge model for $R_{K^{(*)}}$ and aspects of the fermion mass problem*, *JHEP* **12** (2018) 075 [arXiv:1809.01158] [INSPIRE].

[62] B.C. Allanach, T. Corbett, M.J. Dolan and T. You, *Hadron collider sensitivity to fat flavourful Z's for $R_{K^{(*)}}$*, *JHEP* **03** (2019) 137 [arXiv:1810.02166] [INSPIRE].

[63] A. Crivellin, J. Fuentes-Martin, A. Greljo and G. Isidori, *Lepton Flavor Non-Universality in B decays from Dynamical Yukawas*, *Phys. Lett.* **B 766** (2017) 77 [arXiv:1611.02703] [INSPIRE].

[64] J.F. Kamenik, Y. Soreq and J. Zupan, *Lepton flavor universality violation without new sources of quark flavor violation*, *Phys. Rev.* **D 97** (2018) 035002 [arXiv:1704.06005] [INSPIRE].

[65] J.E. Camargo-Molina, A. Celis and D.A. Faroughy, *Anomalies in Bottom from new physics in Top*, *Phys. Lett.* **B 784** (2018) 284 [arXiv:1805.04917] [INSPIRE].

[66] R.S. Chivukula, J. Isaacson, K.A. Mohan, D. Sengupta and E.H. Simmons, *R_K anomalies and simplified limits on Z' models at the LHC*, *Phys. Rev.* **D 96** (2017) 075012 [arXiv:1706.06575] [INSPIRE].

[67] B.C. Allanach, B. Gripaios and T. You, *The case for future hadron colliders from $B \to K^{(*)}\mu^+\mu^-$ decays*, *JHEP* **03** (2018) 021 [arXiv:1710.06363] [INSPIRE].

[68] FCC collaboration, *FCC Physics Opportunities*, *Eur. Phys. J.* **C 79** (2019) 474 [INSPIRE].

[69] ATLAS collaboration, *Search for heavy particles decaying into top-quark pairs using lepton-plus-jets events in proton-proton collisions at $\sqrt{s} = 13$ TeV with the ATLAS detector*, *Eur. Phys. J.* **C 78** (2018) 565 [arXiv:1804.10823] [INSPIRE].

[70] ATLAS collaboration, *Search for heavy particles decaying into a top-quark pair in the fully hadronic final state in pp collisions at $\sqrt{s} = 13$ TeV with the ATLAS detector*, *Phys. Rev.* **D 99** (2019) 092004 [arXiv:1902.10077] [INSPIRE].

[71] ATLAS collaboration, *A search for high-mass resonances decaying to $\tau^+\tau^-$ in pp collisions at $\sqrt{s} = 8$ TeV with the ATLAS detector*, *JHEP* **07** (2015) 157 [arXiv:1502.07177] [INSPIRE].

JHEP08(2019)106

[72] ATLAS collaboration, *Search for high-mass dilepton resonances using* $139\,fb^{-1}$ *of pp collision data collected at* $\sqrt{s} = 13$ *TeV with the ATLAS detector*, *Phys. Lett.* **B 796** (2019) 68 [arXiv:1903.06248] [INSPIRE].

[73] ATLAS collaboration, *Search for high-mass dilepton resonances using* $139\,fb^{-1}$ *of pp collision data collected at* $\sqrt{s} = 13$ *TeV with the ATLAS detector*, *Phys. Lett.* **B 796** (2019) 68 [arXiv:1903.06248] [INSPIRE].

[74] HFLAV collaboration, *Averages of b-hadron, c-hadron and* τ*-lepton properties as of summer 2016*, *Eur. Phys. J.* **C 77** (2017) 895 [arXiv:1612.07233] [INSPIRE].

[75] D. King, A. Lenz and T. Rauh, B_s *mixing observables and* $|V_{td}/V_{ts}|$ *from sum rules*, *JHEP* **05** (2019) 034 [arXiv:1904.00940] [INSPIRE].

[76] L. Di Luzio, M. Kirk and A. Lenz, *Updated* B_s*-mixing constraints on new physics models for* $b \to s\ell^+\ell^-$ *anomalies*, *Phys. Rev.* **D 97** (2018) 095035 [arXiv:1712.06572] [INSPIRE].

[77] C. Degrande, C. Duhr, B. Fuks, D. Grellscheid, O. Mattelaer and T. Reiter, *UFO — The Universal FeynRules Output*, *Comput. Phys. Commun.* **183** (2012) 1201 [arXiv:1108.2040] [INSPIRE].

[78] A. Alloul, N.D. Christensen, C. Degrande, C. Duhr and B. Fuks, *FeynRules 2.0 — A complete toolbox for tree-level phenomenology*, *Comput. Phys. Commun.* **185** (2014) 2250 [arXiv:1310.1921] [INSPIRE].

[79] J. Alwall et al., *The automated computation of tree-level and next-to-leading order differential cross sections and their matching to parton shower simulations*, *JHEP* **07** (2014) 079 [arXiv:1405.0301] [INSPIRE].

[80] M. Lim, F. Maltoni, G. Ridolfi and M. Ubiali, *Anatomy of double heavy-quark initiated processes*, *JHEP* **09** (2016) 132 [arXiv:1605.09411] [INSPIRE].

[81] J.M. Butterworth, D. Grellscheid, M. Krämer, B. Sarrazin and D. Yallup, *Constraining new physics with collider measurements of Standard Model signatures*, *JHEP* **03** (2017) 078 [arXiv:1606.05296] [INSPIRE].

[82] J. Bellm et al., *HERWIG 7.0/HERWIG++ 3.0 release note*, *Eur. Phys. J.* **C 76** (2016) 196 [arXiv:1512.01178] [INSPIRE].

[83] J. Bellm et al., *HERWIG 7.1 Release Note*, arXiv:1705.06919 [INSPIRE].

[84] A. Buckley et al., *Rivet user manual*, *Comput. Phys. Commun.* **184** (2013) 2803 [arXiv:1003.0694] [INSPIRE].

[85] G. Brooijmans et al., *Proceedings of the Les Houches 2017: Physics at TeV Colliders New Physics Working Group Report*, Les Houches, France, 5–23 June 2017, arXiv:1803.10379 [INSPIRE].

[86] S. Amrith, J.M. Butterworth, F.F. Deppisch, W. Liu, A. Varma and D. Yallup, *LHC constraints on a* $B - L$ *gauge model using Contur*, *JHEP* **05** (2019) 154 [arXiv:1811.11452] [INSPIRE].

[87] ATLAS collaboration, *Measurements of inclusive and differential fiducial cross-sections of* $t\bar{t}$ *production with additional heavy-flavour jets in proton-proton collisions at* $\sqrt{s} = 13$ *TeV with the ATLAS detector*, *JHEP* **04** (2019) 046 [arXiv:1811.12113] [INSPIRE].

[88] ATLAS collaboration, *Search for triboson* $W^{\pm}W^{\pm}W^{\mp}$ *production in pp collisions at* $\sqrt{s} = 8$ *TeV with the ATLAS detector*, *Eur. Phys. J.* **C 77** (2017) 141 [arXiv:1610.05088] [INSPIRE].

JHEP08(2019)106

[89] CMS collaboration, *Measurement of differential cross sections for top quark pair production using the lepton + jets final state in proton-proton collisions at* 13 *TeV*, *Phys. Rev.* **D 95** (2017) 092001 [arXiv:1610.04191] [INSPIRE].

[90] ATLAS collaboration, *Measurement of the double-differential high-mass Drell-Yan cross section in pp collisions at* $\sqrt{s} = 8$ *TeV with the ATLAS detector*, *JHEP* **08** (2016) 009 [arXiv:1606.01736] [INSPIRE].

[91] Working Group 3, *Beyond the Standard Model Physics at the HL-LHC and HE-LHC*, arXiv:1812.07831 [INSPIRE].

JHEP08(2019)106